Temperature and magnetic field dependent behavior of atomic-scale skyrmions in Pd/Fe/Ir(111) nanoislands

P. Lindner,* L. Bargsten, S. Kovarik, J. Friedlein, J. Harm, S. Krause,† and R. Wiesendanger
Department of Physics, University of Hamburg, 20355 Hamburg, Germany

(Received 1 October 2019; revised manuscript received 3 June 2020; accepted 8 June 2020; published 30 June 2020)

The thermal stability of atomic-scale skyrmions is of high relevance for potential spintronics applications and validation of theoretical models. We investigated Pd/Fe nanoislands on an Ir(111) substrate as a function of temperature and magnetic field. Utilizing noncollinear magnetoresistance contrast in scanning tunneling microscopy, the thermomagnetic phase space is explored up to 3 T within a temperature range between 1 K to 100 K. Evidence is found for the spin spiral, field-polarized, and fluctuating disordered magnetic phases. Evidence for the presence of atomic-scale skyrmions at up to approximately 80 K is found, irrespective of considerable magnetization dynamics arising from thermal agitation.

DOI: 10.1103/PhysRevB.101.214445

Material systems with broken inversion symmetry, such as metallic surfaces or interfaces [1–5] or certain noncentrosymmetric crystals [6–8], can host chiral magnetic skyrmions that offer great potential for future data storage and processing technology. Due to their special topological structure resulting from competing Dzyaloshinskii-Moriya interaction [9,10], magnetic exchange, and magnetocrystalline anisotropy, skyrmions are hindered to decay into the ferromagnetic state by activation energy barriers and therefore exhibit high stability against external magnetic fields and temperature. Atomic-scale skyrmions with diameters below 10 nm are potential candidates to compete with current magnetic domain-based storage media, paving the path towards ultradense storage media and high speed processing devices, such as skyrmion racetrack memories and logic gates [11–13].

Preparing a single atomic layer of Fe on an Ir(111) substrate results in the formation of a nanoskymion lattice with a unit cell of approx. 1 nm [2]. It exhibits stability against thermal agitation up to 28 K [14]. Capping the system with an atomic layer of Pd results in the formation of atomic-scale spin spirals which can be transformed into skyrmions with a diameter well below 10 nm, utilizing an external magnetic field [1]. These skyrmions were shown to be individually generated and annihilated using the magnetic tip of a spin-polarized scanning tunneling microscope (SP-STM). Additional manipulation techniques are used to control the size and the shape of the skyrmions via magnetic field tuning [15] and to stabilize skyrmions by local pinning to surface defects like adatoms or atomic step edges [16]. Consequently, the Pd/Fe/Ir(111) system qualifies as a potential candidate for future magnetic storage applications in terms of feature size and manipulation capabilities. Compared to the uncapped Fe/Ir(111) system, theoretical investigations raise expectations for an increased thermal stability of the skyrmion phase, attributed to strong exchange interactions between the Fe atoms and the highly polarizable, almost ferromagnetic Pd atoms [17] and entropic stabilization [18]. So far, experiments on skyrmions in this system have been limited to temperatures T below 10 K. To understand the basic mechanisms for the stabilization of skyrmions and to identify sample systems that host atomic-scale skyrmions at elevated T, it is crucial to elaborate the thermomagnetic phase diagram over a wide temperature and magnetic field range.

In our experimental approach, we use an STM setup that allows for the application of external magnetic fields of up to $B = 3$ T at variable T, with $1.2\ \mathrm{K} \leqslant T \leqslant 100$ K. Performing scanning tunneling microscopy and spectroscopy we identify parameters of T and B that stabilize atomic-scale skyrmions in the Pd/Fe/Ir(111) system. The experiments were conducted in a home-built STM located in the center of a cryostat inside an ultrahigh vacuum chamber system with satellite chambers for dedicated sample cleaning and molecular beam epitaxy [19]. A superconducting split-pair magnet generates magnetic fields of up to 3 T perpendicular to the sample plane. The STM is mounted on a 1 K pot with additional pumping, thereby realizing a base temperature down to 1.2 K. The connection between the 1 K pot and the bath cryostat is realized by thin metal struts with limited heat transfer. This low thermal coupling to the bath cryostat in combination with resistive heating of the sample allows STM studies at variable temperature, while the split coils for the generation of the magnetic field remain in the superconducting state. The Ir(111) substrate was cleaned by repeated cycles of argon ion sputtering and oxygen annealing [1]. After a final step of flash annealing nominally <0.5 monolayer (ML) Fe at 525 K and <0.2 ML Pd at 375 K were deposited by electron beam evaporators at a background pressure below 1×10^{-9} mbar. For the STM experiments an electrochemically etched bulk Cr tip was used that was prepared *in situ* by high voltage pulses to

*plindner@physnet.uni-hamburg.de
†skrause@physnet.uni-hamburg.de

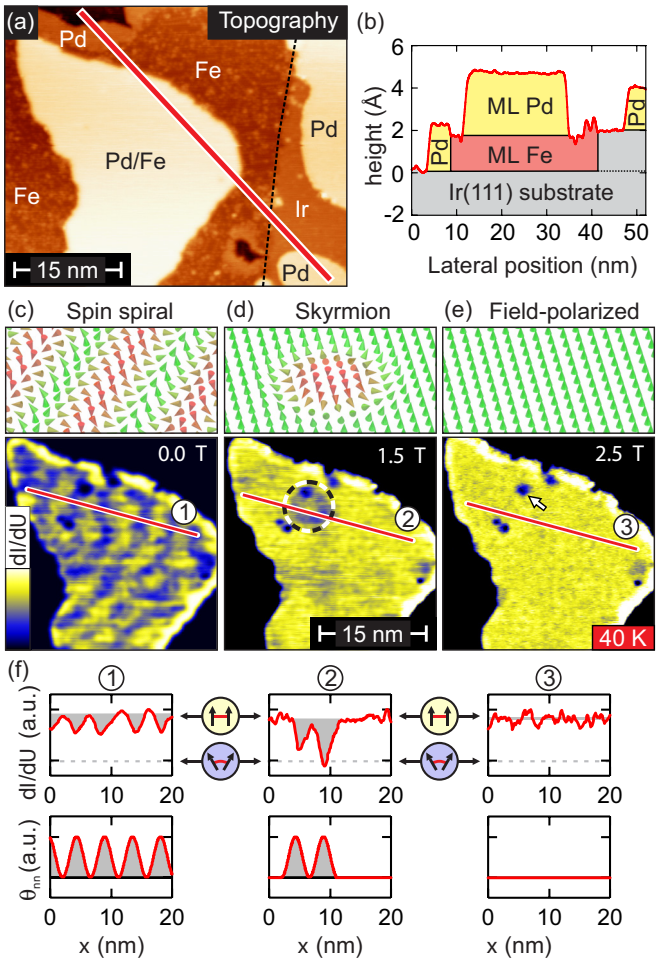

FIG. 1. (a) Constant current STM image of the Pd/Fe/Ir(111) sample. A step edge of the Ir(111) substrate, preferentially aligning along $[\bar{1}10]$ or equivalent directions, is indicated by the dashed line. (b) Line profile along the red line in (a) for the determination of the sample structure in terms of substrate and atomic layers of Fe and Pd, respectively. (c)–(e) Top: Spin texture schematics of the spin spiral, skyrmion, and field-polarized state. Bottom: dI/dU maps taken on the Pd island at $B = 0$ T, $B = 1.5$ T, and $B = 2.5$ T, respectively. A pinning center for skyrmions is marked by the arrow. (f) Line profiles taken along the lines in (c)–(e) (top) and schematics of neighboring spin canting angle θ_{nn} (bottom) for the three different phases, respectively. The dI/dU signal gives a measure of local noncollinearity, as indicated by the gray shading. $I = 1$ nA, $U = 700$ mV.

remove potential oxide layers [20]. Images were generated by scanning the biased tip over the sample surface at constant tunnel current, while simultaneously recording the differential tunneling conductance dI/dU via lock-in technique ($U_{mod} = 40$ mV).

A typical sample topography is shown in Fig. 1(a), together with a line profile in Fig. 1(b). The surface of the Ir(111) substrate exhibits extended atomically flat terraces separated by monoatomic step edges. Evaporating Fe results in the step-flow growth of extended fcc-Fe MLs. Subsequent evaporation of Pd leads to ML islands in fcc and bcc stacking on top of the Fe/Ir(111) surface. Our study focuses on the noncollinear spin texture of the Pd islands in fcc stacking. This system has been investigated intensively both by experimental as well as theoretical approaches [1,15–18,21–26]. The fcc-stacked Pd islands were identified analyzing dI/dU maps at a bias $U = 700$ mV and tunnel current setpoint $I = 1$ nA.

I. NCMR IMAGING OF THE ORDERED PHASES

In our experiments we utilize the noncollinear magnetoresistance (NCMR) between the (nonmagnetic) tip and the surface as a measure for the noncollinearity of the Pd/Fe/Ir(111) spin texture. NCMR originates from the canting of neighboring surface spins that result in a mixing between spin-up and spin-down tunneling channels [23]. For 600 mV $\leqslant U \leqslant$ 800 mV, this NCMR contrast, as measured by the dI/dU signal, is maximized. A high dI/dU signal corresponds to highly collinear spins, and it decreases with increasing noncollinearity. Consequently, recording dI/dU while scanning the surface results in maps of local spin collinearity. In Figs. 1(c)–1(e), such dI/dU maps of the Pd/Fe nanoisland shown in Fig. 1(a) are shown for three different setpoints of B at $T = 40$ K. In the absence of an external magnetic field, a stripe pattern is visible in Fig. 1(c), which originates from the magnetic ground state, being an inhomogeneous spin spiral with a period between 6 and 7 nm [1]. In agreement with the observed pattern, half of the spiral period is expected to be seen in NCMR contrast images.

When increasing B, the spin spiral phase transforms into a phase with individual skyrmions embedded in a field-polarized background [1]. In Fig. 1(d), a dI/dU map is shown, taken at $B = 1.5$ T on the same nanoisland. The island exhibits an almost homogeneous high signal. A ring-shape feature of low signal intensity is observed, as indicated by the dashed circle. It corresponds to a single skyrmion that is hosted in the otherwise field-polarized nanoisland. In NCMR maps taken at intermediate values of B, skyrmions appear ring shaped, as the maximum canting between adjacent spins occurs on the circularly shaped set of inflection points around the skyrmion center [15]. Skyrmions in this system are found to pin at inhomogeneities like in-layer defects or adatoms, arising from the modification of local magnetic interactions [16]. Likewise, such a pinning center is visible as a dark spot in the dI/dU map, marked by the arrow in Fig. 1(e). In Fig. 1(e), the dI/dU map is shown for $B = 2.5$ T. At this field strength, the skyrmion feature has vanished, resulting in an island with a homogeneous bright dI/dU signal, despite some very small local variations. These spots correspond to individual defect atoms that locally modify the electronic structure, i.e., the local density of states, and thereby affect the dI/dU signal, irrespective of NCMR. The island is found to be fully field-polarized, hosting no noncollinear spin textures like spin spirals or skyrmions. To clarify the assignment of features in the dI/dU maps, line profiles are taken along the lines indicated in Figs. 1(c)–1(e) and shown in Fig. 1(f), respectively. For an inhomogeneous spin spiral, the dI/dU signal varies with a period of half the magnetic period, corresponding to the variation of the nearest-neighbor spin canting angle θ_{nn}. A skyrmion is identified by a set of two dips in the dI/dU line profile, corresponding to the two spots of maximized noncollinearity in terms of θ_{nn} across this

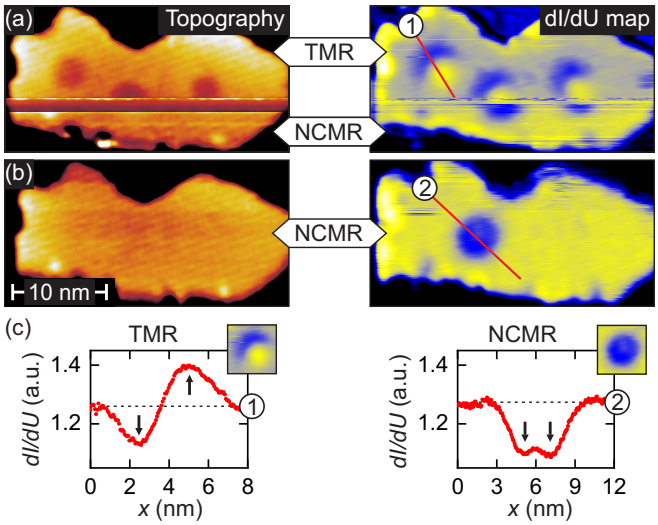

FIG. 2. TMR and NCMR imaging techniques. (a) Constant-current topography (left) and dI/dU map (right) of a Pd/Fe nanoisland recorded during an accidental tip change leading to a switching between the TMR (top) and NCMR contrast imaging (bottom). (b) Same nanoisland, solely recorded with NCMR contrast. (c) Skyrmion line profiles along red lines in (a) and (b). Based on TMR, a two-lobe structure is found (left), whereas a diplike feature is observed with NCMR contrast (right). $I = 1$ nA, $U = 700$ mV, $B = 1.5$ T, $T = 1.2$ K.

spin texture. Away from the skyrmion, the dI/dU signal is high, indicating a field-polarized collinear spin alignment. For high B, a homogeneously bright dI/dU signal is observed, indicating the absence of local noncollinearity. From the maps in Fig. 1 taken at $T = 40$ K we identify the same three phases in the Pd/Fe islands that were found in earlier experiments on extended films at $T < 10$ K [1]. Our experiments demonstrate their existence on the nanoislands, even at elevated temperatures of $T = 40$ K.

II. DISCRIMINATION BETWEEN THE NCMR AND TMR IMAGING MODES

Conventionally, Cr bulk tips serve as scanning probes for SP-STM experiments utilizing the tunneling-magnetoresistance (TMR) effect [20]. In Fig. 2, magnetic imaging is demonstrated on an individual Pd/Fe nanoisland. An accidental tip change occurred that switched between TMR and NCMR contrast imaging in the topography as well as in the dI/dU channels. In the upper part of the image of Fig. 2(a), the condition of the Cr tip is such that it leads to a TMR contrast. Three faint depressions of approximately 7 pm in the constant-current topography channel indicate the presence of individual skyrmions. In the dI/dU map, lobelike structures are found at their positions. Both findings are in good agreement with previous studies utilizing a significant spin polarization of the tunnel current [1]. In the lower part of the image, the tip changed to the NCMR imaging mode. Here, no indications of skyrmions are found in the constant-current topography channel. However, dark features are found in the dI/dU map at the positions of the skyrmions. In Fig. 2(b), the same nanoisland was investigated again, now using the tip in a stable state for NCMR-based imaging. Whereas the topography of the nanoisland appears featureless, a dark spot in the dI/dU map indicates the presence of an individual skyrmion. Two line profiles of the dI/dU maps across individual skyrmions are shown in Fig. 2(c), recorded in the TMR and NCMR imaging mode, respectively. TMR contrast results in a profile that is characterized by a depression and protrusion [Fig. 2(c), left]. Obviously, the Cr tip has a strong in-plane magnetization component, so that the relative spin alignment between the STM tip and the skyrmion rotates continuously from antiparallel to parallel while scanning across the skyrmion. This results in a spin-polarized dI/dU signal that is characterized by a depression followed by a protrusion. Hence, the skyrmion appears as a lobelike structure in the spin-resolved dI/dU map, although the skyrmion spin texture is rotationally symmetric [1]. On the other hand, NCMR contrast yields a diplike feature in the dI/dU image. The rotational symmetry of the skyrmion is reflected by the circular shape of the observed feature. On closer inspection of the line profile [Fig. 2(c), right], two separated local minima are identified within the dip. They correspond to the maxima of noncollinearity at each side of the skyrmion. With increasing B field the skyrmion shrinks, thereby driving the two local minima toward the center of the skyrmion [23]. Measuring the constant-current topography and dI/dU map of magnetic nanoislands with noncollinear spin textures therefore allows a distinction between the TMR and NCMR contrast mechanisms. In our present study, the tunnel current did not exhibit significant contributions of TMR contrast. Consequently, we utilized the NCMR imaging mode for revealing the spatial distributions of noncollinear spin textures.

III. THERMALLY DRIVEN SKYRMION DYNAMICS

Although the dI/dU maps of Fig. 1 are in good agreement with the experiments in Ref. [1], there are significant differences in the experimental results, originating from thermally driven magnetization dynamics at elevated T. In Figs. 3(a) and 3(b), the topography and the simultaneously obtained dI/dU map on a Pd/Fe island are shown, respectively. Two disk shaped areas are visible that exhibit dark stripes. They arise from two skyrmions that are frequently nucleated and annihilated by the electric field between the biased tip and the sample [1]. The stripe pattern localized at the position of the switching skyrmion indicates that the skyrmion lifetime is on the timescale of the scanning, i.e., on the order of seconds. Parking the probe tip above the skyrmion and recording the temporal evolution of the dI/dU signal results in a telegraphic noise, as shown in the inset of Fig. 3(c). Here, the signal jumps between high and low levels, corresponding to low and high NCMR and indicating the absence ("0") or presence ("1") of a skyrmion. Performing a detailed telegraph noise analysis [1,27] for different T between 1.6 K and 7.0 K yields the annihilation rate shown in the Arrhenius plot in Fig. 3(c). The annihilation rate stays almost constant for $T < 3$ K. Consequently, the switching behavior is dominated by the electric field, and the effects of thermal agitation are negligible. A rapid increase of the switching rate with T is observed for $T > 3$ K, indicating dynamic processes that

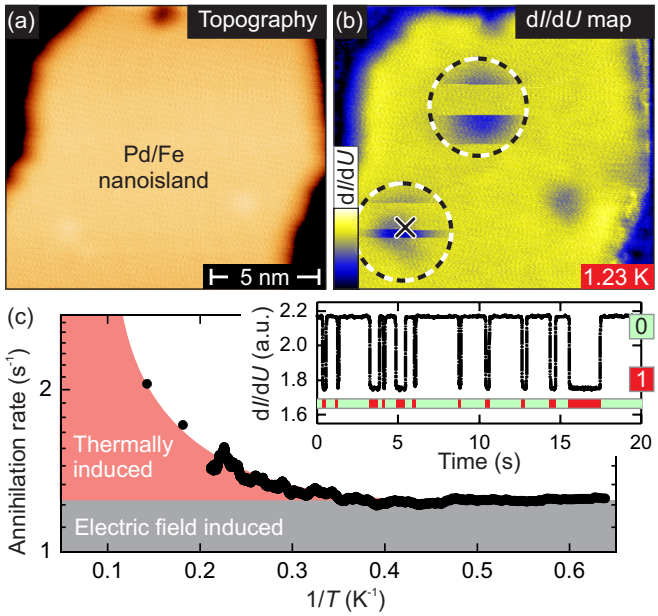

FIG. 3. Skyrmion creation and annihilation dynamics. Topography map of a Pd/Fe nanoisland (a) and simultaneously recorded dI/dU map (b). Skyrmion positions within the field-polarized nanoisland are marked by dotted circles. The presence of a skyrmion is indicated by a low signal (dark features). $I = 1$ nA, $U = 700$ mV, $B = 2.5$ T. (c) Arrhenius plot of the skyrmion annihilation rate derived from the telegraphic noise (inset) recorded at the position indicated by the cross in (b). "1" ("0") denotes the presence (absence) of a skyrmion. $I = 10$ nA, $U = 700$ mV, $B = 2.5$ T.

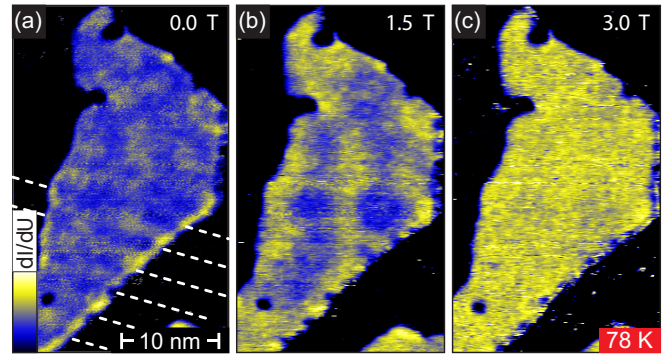

FIG. 4. Magnetic-field dependent dI/dU maps of a Pd/Fe nanoisland at $T = 78$ K. (a) $B = 0$ T: Indications for the existence of a spin spiral are found in the lower part (striped lines), whereas irregular, disordered structures are visible in the upper part of the nanoisland. (b) $B = 1.5$ T: Bright areas evolve, indicating field-polarized regions. Blurred trajectories of skyrmions (dark regions) are visible, with dark spots representing high local dwell time. (c) $B = 3.0$ T: The nanoisland is almost completely field polarized, resulting in an almost homogeneous high signal. $I = 1$ nA, $U = 700$ mV.

are predominantly driven by thermal agitation, rather than electric-field-driven dynamics. For $T \geqslant 30$ K, the skyrmion generation and annihilation rates exceed the temporal resolution of the transimpedance amplifier, and no individual switching events are observed. The dI/dU maps taken at elevated T are thus considered to be time averaged. In view of this fact, Figs. 1(c)–1(e) have to be interpreted as maps of the probability distribution of noncollinearity, and local blurring indicates a possible instability or lateral motion of the respective spin texture. Note that the skyrmions in Fig. 3(b) appear as dark dots rather than ring shaped. This is a consequence of the high magnetic field of $B = 2.5$ T which induces a considerable shrinking of the skyrmion, resulting in a transformation of the NCMR contrast feature from a ring to a single dot [23].

In Fig. 4, dI/dU maps of a different Pd/Fe nanoisland are shown, investigated at $T = 78$ K. Here, indications for the presence of a spin spiral in the absence of a magnetic field can be found, as shown in Fig. 4(a). However, a significant part of the nanoisland exhibits a fuzzy pattern, with no clear evidence for a spin spiral. The overall low signal in this area implies a high degree of (time-averaged) spin noncollinearity. At a moderate magnetic field of $B = 1.5$ T, inhomogeneities in the dI/dU signal evolve on the nanoisland, as shown in Fig. 4(b). Here, areas of high and low spin collinearity coexist. In this regime of T and B, we interpret this finding in terms of highly dynamic skyrmions that are no longer pinned to defect sites and therefore move almost freely. In a recent theoretical study, the effect of high mobility on time-averaged imaging of skyrmions was addressed by means of Monte Carlo simulations [26]. Time averaging results in blurred skyrmion trajectories which are in very good agreement with our experimental data. Consequently, skyrmions are present in the Pd/Fe island at $B = 1.5$ T and $T = 78$ K but are highly mobile and lead to the dI/dU map of Fig. 4(b), with pronounced dark spots as indications of local high dwell time. When increasing B to 3.0 T, the nanoisland is driven into the field-polarized state without hosting any skyrmions, resulting in the homogeneous and high dI/dU signal shown in Fig. 4(c).

IV. HIGH-TEMPERATURE DISORDERED STATE

For T above approximately 80 K, the spin texture on the Pd/Fe islands becomes very irregular. A typical series of B dependent dI/dU maps in this regime is shown in Fig. 5 for $T = 90$ K. In zero field, the nanoisland appears dark, indicating a high degree of spin noncollinearity. With increasing B, a general trend of brightening is observed, indicating the gradual alignment of atomic spins in the field, resulting in enhanced spin collinearity in the nanoisland. Upon closer inspection, an irregular fine structure is visible. It gradually fades away with increasing B, except for some residual spots at $B = 3$ T. Irrespective of B, no evidence for a spin spiral, skyrmion or fully field-polarized state is found.

In theoretical studies a fluctuating disordered state was found for extended Pd/Fe/Ir(111) films in this regime of elevated T [21,22]. It is characterized by numerous small patches of noncollinear spin textures that frequently nucleate, propagate, and annihilate, with no characteristic feature sizes or shapes. We attribute our experimental observations to such a disordered state in the nanoisland, with short-lived patches of noncollinearity driven by thermal agitation. The

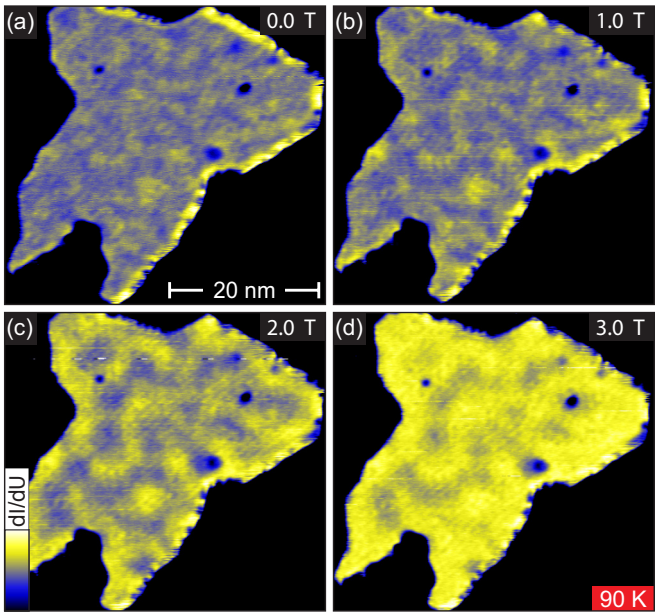

FIG. 5. Magnetic-field dependent dI/dU maps of a Pd/Fe nanoisland at $T = 90$ K and (a) $B = 0$ T, (b) $B = 1$ T, (c) $B = 2$ T, and (d) $B = 3$ T. The fuzzy pattern indicates a disordered spin phase. With increasing magnetic field, an overall increase of the signal intensity evolves, and parts of the dark features disappear, indicating that the magnetic field drives the nanoisland into the field-polarized state. $I = 1$ nA, $U = 700$ mV.

fuzzy dI/dU map arises from the fluctuation dynamics on a timescale that is much shorter than the time resolution in our experiments. Due to the time-averaging nature of the imaging, the spatially-resolved dI/dU signal corresponds to maps of the probability for individual spin sites being in a collinear (high signal) or noncollinear (low signal) configuration with respect to their local surrounding. At $B = 0$ T, the whole nanoisland is in a highly noncollinear state, as indicated by the overall dark appearance in Fig. 5(a). With increasing B, local spin patches are aligned in the magnetic field, as indicated by individual dark spots in Fig. 5(b). At $B = 2$ T, these patches become more pronounced, while the irregular fine structure still persists, as shown in Fig. 5(c). For $B = 3$ T, the nanoisland is in an almost field-polarized state, with local areas exhibiting remains of the fluctuating disordered state, as can be seen from Fig. 5(d).

V. THERMOMAGNETIC PHASE DIAGRAM

To identify parameter sets of T and B that allow for the formation of skyrmions, we systematically analyzed dI/dU maps on Pd/Fe nanoislands. For this study, numerous nanoislands have been evaluated in terms of their spin phase and presence of skyrmions, following the protocols described above. The results are shown in Fig. 6. In the diagram, three areas can be separated from each other. For $T < 80$ K, two different spin phases are stabilized on the nanoislands: The spin spiral phase for $B < 1$ T, and the field-polarized ferromagnetic phase for $B > 1$ T. At $T > 80$ K, a fluctuating disordered phase is revealed, irrespective of B. Indications for the presence of skyrmions are found in a pocket roughly

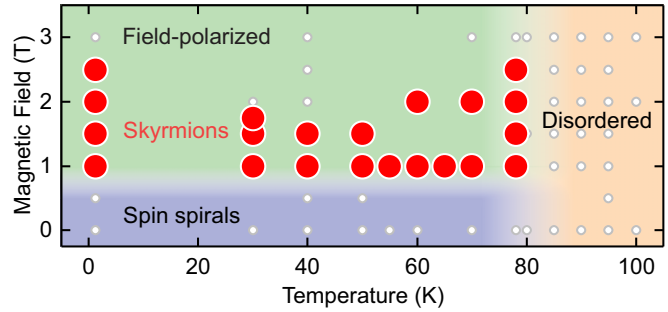

FIG. 6. Thermomagnetic phase diagram of the Pd/Fe nanoislands. Every data point represents investigations for the respective magnetic field and temperature values. The spin spiral, field-polarized, and fluctuating disordered phases are found (color shading). Red data points indicate the existence of skyrmions. $I = 1$ nA, $U = 700$ mV.

confined by 1.0 T $< B <$ 2.5 T and $T < 80$ K, as indicated by the red data points in Fig. 6. The experiments give no evidence for the presence of skyrmions at $T > 80$ K. Theoretical investigations showed the appearance of skyrmions is limited by temperature, in agreement with our results [21,22]. From our experiments, the critical temperature is approximately 80 K. Our experimental results agree well with theoretically derived phase diagrams from Monte-Carlo simulations on extended Pd/Fe/Ir(111) films, yielding a critical temperature for the transition into the disordered spin phase between 81 K [21] and 100 K [22] .

VI. CONCLUSIONS

In summary, we report on the first systematic study of the B and T phase space for the presence of atomic-scale skyrmions in the system of ultrathin Pd/Fe films on Ir(111). Our experimental setup allows for STM experiments covering a wide temperature and magnetic field range. Using the NCMR imaging method, maps of local spin collinearity are obtained on individual Pd/Fe/Ir(111) nanoislands that allow for the assignment of spin textures like spin spirals, skyrmions, or field-polarized order. Skyrmions are found at temperatures up to 80 K and in external magnetic fields between 1 T and 2.5 T. Compared to the system of Fe/Ir(111) without Pd capping, the critical temperature is increased by a factor three. Hence, our study demonstrates the stabilization of atomic-scale skyrmions against thermal agitation by adding an atomic layer of a highly polarizable elements. Together with theoretical investigations, our experimental approach allows for a detailed understanding of the underlying physics of noncollinear magnetism, paving the way for the tailoring of ultrathin film systems that host atomic-scale skyrmions, potentially even at room temperature.

ACKNOWLEDGMENTS

Financial support was provided by the Deutsche Forschungsgemeinschaft (DFG) via Grant No. SPP2137 (Skyrmionics) and the SFB925, part project B9.

[1] N. Romming, C. Hanneken, M. Menzel, J. E. Bickel, B. Wolter, K. von Bergmann, A. Kubetzka, and R. Wiesendanger, Science **341**, 636 (2013).
[2] S. Heinze, K. von Bergmann, M. Menzel, J. Brede, A. Kubetzka, R. Wiesendanger, G. Bihlmayer, and S. Blügel, Nat. Phys. **7**, 713 (2011).
[3] S. Woo, K. Litzius, B. Krüger, M.-Y. Im, L. Caretta, K. Richter, M. Mann, A. Krone, R. M. Reeve, M. Weigand, P. Agrawal, I. Lemesh, M.-a. Mawass, P. Fischer, M. Kläui, and G. S. D. Beach, Nat. Mater. **15**, 501 (2016).
[4] P. J. Hsu, A. Kubetzka, A. Finco, N. Romming, K. von Bergmann, and R. Wiesendanger, Nat. Nanotechnol. **12**, 123 (2017).
[5] P. J. Hsu, L. Rózsa, A. Finco, L. Schmidt, K. Palotás, E. Vedmedenko, L. Udvardi, L. Szunyogh, A. Kubetzka, K. von Bergmann, and R. Wiesendanger, Nat. Commun. **9**, 1571 (2018).
[6] X. Z. Yu, Y. Onose, N. Kanazawa, J. H. Park, J. H. Han, Y. Matsui, N. Nagaosa, and Y. Tokura, Nature (London) **465**, 901 (2010).
[7] S. Seki, X. Z. Yu, S. Ishiwata, and Y. Tokura, Science **336**, 198 (2012).
[8] S. Mühlbauer, B. Binz, F. Jonietz, C. Pfleiderer, A. Rosch, A. Neubauer, R. Georgii, and P. Böni, Science **323**, 915 (2009).
[9] I. Dzyaloshinskii, J. Phys. Chem. Solids **4**, 241 (1958).
[10] T. Moriya, Phys. Rev. **120**, 91 (1960).
[11] A. Fert, V. Cros, and J. Sampaio, Nat. Nanotechnol. **8**, 152 (2013).
[12] X. Zhang, G. P. Zhao, H. Fangohr, J. P. Liu, W. X. Xia, J. Xia, and F. J. Morvan, Sci. Rep. **5**, 7643 (2015).
[13] S. Krause and R. Wiesendanger, Nat. Mater. **15**, 493 (2016).
[14] A. Sonntag, J. Hermenau, S. Krause, and R. Wiesendanger, Phys. Rev. Lett. **113**, 077202 (2014).
[15] N. Romming, A. Kubetzka, C. Hanneken, K. von Bergmann, and R. Wiesendanger, Phys. Rev. Lett. **114**, 177203 (2015).
[16] C. Hanneken, A. Kubetzka, K. von Bergmann, and R. Wiesendanger, New J. Phys. **18**, 055009 (2016).
[17] B. Dupé, M. Hoffmann, C. Paillard, and S. Heinze, Nat. Commun. **5**, 4030 (2014).
[18] J. Hagemeister, N. Romming, K. Von Bergmann, E. Y. Vedmedenko, and R. Wiesendanger, Nat. Commun. **6**, 8455 (2015).
[19] J. Friedlein, J. Harm, P. Lindner, L. Bargsten, M. Bazarnik, S. Krause, and R. Wiesendanger, Rev. Sci. Instrum. **90**, 123705 (2019).
[20] A. Schlenhoff, S. Krause, G. Herzog, and R. Wiesendanger, Appl. Phys. Lett. **97**, 083104 (2010).
[21] M. Böttcher, S. Heinze, S. Egorov, J. Sinova, and B. Dupé, New J. Phys. **20**, 103014 (2018).
[22] L. Rózsa, E. Simon, K. Palotás, L. Udvardi, and L. Szunyogh, Phys. Rev. B **93**, 024417 (2016).
[23] C. Hanneken, F. Otte, A. Kubetzka, B. Dupé, N. Romming, K. von Bergmann, R. Wiesendanger, and S. Heinze, Nat. Nanotechnol. **10**, 1039 (2015).
[24] P. F. Bessarab, G. P. Müller, I. S. Lobanov, F. N. Rybakov, N. S. Kiselev, H. Jónsson, V. M. Uzdin, S. Blügel, L. Bergqvist, and A. Delin, Sci. Rep. **8**, 3433 (2018).
[25] S. von Malottki, P. F. Bessarab, S. Haldar, A. Delin, and S. Heinze, Phys. Rev. B **99**, 060409(R) (2019).
[26] A. Schäffer, L. Rózsa, J. Berakdar, E. Y. Vedmedenko, and R. Wiesendanger, Commun. Phys. **2**, 72 (2019).
[27] S. Krause, G. Herzog, A. Schlenhoff, A. Sonntag, and R. Wiesendanger, Phys. Rev. Lett. **107**, 186601 (2011).